Scientific Research Publishing

World Journal of Engineering and Technology, 2025, 13(1), 64-79
https://www.scirp.org/journal/wjet
ISSN Online: 2331-4249
ISSN Print: 2331-4222

Study on the Safety Influence of the Shield Tunnel under Through Construction of an Existing Intercity Railway Structure

Yue Yang

China Railway Design Corporation, Tianjin, China
Email: yangyue@crdc.com

How to cite this paper: Yang, Y. (2025) Study on the Safety Influence of the Shield Tunnel under Through Construction of an Existing Intercity Railway Structure. *World Journal of Engineering and Technology*, **13**, 64-79.
https://doi.org/10.4236/wjet.2025.131005

Received: December 10, 2024
Accepted: February 11, 2025
Published: February 14, 2025

Abstract

The construction of the new tunnel under the existing railway will break the original stress balance in the engineering area, resulting in the secondary redistribution of surrounding rock stress. The large amount of excavation unloading of the soil below is also easy to induce the uneven settlement deformation of the existing structure above, affecting the safety of driving. Based on the shield tunnel project between Caoqiao Station and Lize Business District Station of Beijing Metro, this paper restores the construction site by constructing the finite element numerical model of the project area, calculates and analyzes the deformation and stress of the existing railway structure before and after the construction of the tunnel, and determines the safety impact of the new structure on the existing railway. The results show that the shield tunnel undercrossing construction will cause the "concave" settlement of the railway subgrade above. Under the condition of grouting reinforcement, the "concave" settlement curve is slower and the distribution range is wider. With the advancement of the construction step, the settlement deformation of the subgrade gradually increases. When the tunnel approaches and passes directly below the subgrade, the settlement deformation curve of the subgrade changes from slow to steep. After the tunnel passes away, the curve changes from steep to slow, and the deformation of the subgrade reaches the maximum after the tunnel is connected. Under the grouting condition, the maximum settlement deformation of the subgrade is 2.08 mm, which is about 45% of the settlement deformation of the subgrade under the non-grouting condition. The ground grouting reinforcement can effectively control the subgrade settlement, and the field monitoring verifies the rationality of the calculation results. After the tunnel passes underneath, the most unfavorable section of the existing railway frame bridge is located at the top plate of the structure, and the maximum crack width is 0.178 mm. After grouting reinforcement, the stress environment

of the structure is improved, the crack width generated by the structure is smaller, the reinforcement area required for calculation is less, and the structural safety meets the requirements.

Keywords

Shield Tunnel, Under Through, Existing Railway, Numerical Calculation, Structural Safety Analysis

1. Introduction

As the transportation industry continues to develop rapidly, adjacent construction projects are increasingly common [1]-[3]. One such project involves constructing new tunnels beneath existing roadbeds, which disrupts the original stress equilibrium in the area. The additional stress from tunnel construction alters the stress distribution within the existing roadbed structure, potentially compromising its stability. Furthermore, extensive excavation and unloading of the underlying soil can lead to uneven settlement and deformation of the overlying roadbed, posing significant risks to driving safety [4]-[6].

Yueguang Song [7] conducted a study integrating numerical simulations and on-site monitoring to assess the effects of subway shield tunnel undercrossing on the settlement deformation of high-speed railway subgrades. The findings suggest that when the shield tunnel's burial depth exceeds three times its diameter, the impact on subgrade settlement is negligible. Wu *et al.* [8] developed a three-dimensional refined finite element model for a double-line shield tunnel undercrossing the Xu-Lan high-speed railway, simulating the construction site to analyze the subgrade settlement deformation during the tunnel undercrossing phase and examining the influence of CFG pile reinforcement on subgrade settlement. Song *et al.* [9] employed a combination of laboratory model tests, numerical simulations, and empirical analysis to investigate the deformation effects of new tunnel undercrossing on existing railway subgrades. Huang *et al.* [10] identified optimal tunneling parameters for shield machines undercrossing existing railway subgrade sections through field experiments. Wang [11] established standards for controlling settlement of railway beds and tracks, considering the engineering characteristics of shallow-buried and concealed excavation of double-arch tunnels in loess strata. Zheng [12] focused on the Jiulong River cross-railway water diversion tunnel in Fujian Province, utilizing the FLAC3D large-scale finite difference software to analyze the impact of tunnel construction on the existing subgrade structure above under various conditions. The research indicates that the maximum subgrade settlement occurs directly above the tunnel centerline.

In summary, there are numerous scholars have conducted extensive research on the construction of tunnels beneath existing roadbeds using various methods such as numerical calculations and on-site monitoring, achieving significant research outcomes. The construction of tunnels beneath existing structures has led

to settlement deformation of the roadbed, affecting the operational safety of existing railways and making the evaluation of the structural safety of existing railways particularly important. However, there is currently limited research on the safety evaluation of tunnel underpass roadbed construction. This paper takes the example of the shield tunnel section between Caoqiao Station and Lize Business District Station of the Beijing Metro, which passes beneath the Beijing-Xiong'an Intercity Railway. By constructing a three-dimensional finite element numerical model of the engineering area to simulate the construction site, the study calculates and analyzes the deformation and stress of the existing railway structure before and after tunnel construction, determining the safety impact of the new structure on the existing railway.

2. Project Overview

The tunnel section between Caoqiao Station and Lize Business District Station on Beijing's New Airport Line extends approximately 2475 meters and is constructed using a combination of shield tunneling, open-cut, and mining methods. The shield tunneling portion spans roughly 2211 meters, featuring shield segments with an outer diameter of 8.8 meters, a thickness of 0.45 meters, and a ring width of 1.6 meters, utilizing a staggered joint assembly technique. As depicted in Figure 1, the shield tunneling section is designed to pass beneath the Beijing-Xiong Intercity Railway, forming a horizontal intersection angle of 87.6˚, with a vertical clearance of 25.5 meters from the railway subgrade and 17.8 meters from the railway frame bridge.

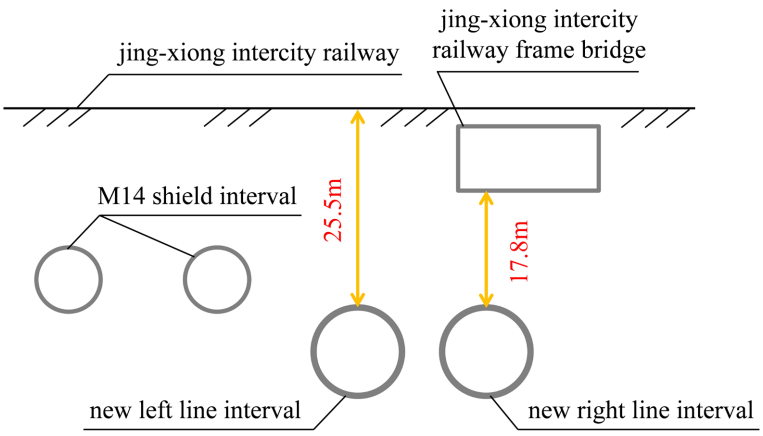

Figure 1. Spatial location relationships.

3. Safety Assessment Standards

3.1. Railway Subgrade Control Standards

The Beijing-Xiong'an Intercity Railway is designed for a speed of 120 km/h and utilizes a ballasted track structure. By referencing safety protection control standards for similar projects domestically and internationally that involve existing railway tunnel underpasses, and integrating existing design and construction experience,

recommended control standard values for this project have been determined. Considering the 100-year service life of the Beijing-Xiong'an Intercity Railway, the control standards for a 120 km/h track structure, as stipulated in the "Rules for Repair of Conventional Railway Lines" (TG/GW102-2019) and the "Technical Regulations for Safety Monitoring of Construction Near Operating Railway Lines" (TB10314-2021), are presented in Table 1.

Table 1. Standards for controlling indicators associated with the Beijing-Xiong'an intercity railway.

Parameter	Warning Value	Alarm Value	Control Value
Subgrade Vertical Displacement	±6 mm	±8 mm	±10 mm
Track Vertical Displacement	+1.8 mm −4.8 mm	+2.4 mm −6.4 mm	+3 mm −8 mm

3.2. Frame Bridge Control Standards

Frame Bridge Control Standards

The frame bridge structure utilizes high-grade concrete. In accordance with the "Code for Design of Concrete Structures" (GB 50010-2010), an analysis is conducted on the deformation limit values of the structure based on the permissible stress levels of the concrete. The approach of "allowable deformation during the construction phase = ultimate state value − reserved redundancy for long-term operation" is employed. Additionally, insights from similar domestic projects are considered to establish the safety control standards for the frame bridge in this project, as detailed in Table 2.

Table 2. Standards for monitoring cracks and vertical displacement in frame bridges.

Parameter	Warning Value	Alarm Value	Control Value
Cracks in Frame Bridges	/	/	0.2 mm
Vertical Displacement in Frame Bridges	±3 mm	±4 mm	±5 mm

The crack width in reinforced concrete components is determined using Equation (1):

$$\omega_{\max} = \alpha_{cr}\psi\frac{\sigma_s}{E_S}\left(1.9c_s + 0.08\frac{d_{eq}}{\rho_{te}}\right) \quad (1)$$

In the equation: $\omega_{\max}$ represents the maximum crack width of the structure, measured in millimeters (mm); ψ denotes the non-uniformity coefficient for the strain of longitudinal tensile reinforcement between cracks; σ_s indicates the tensile stress experienced by the reinforced concrete structure, expressed in megapascals (MPa); E_S refers to the elastic modulus of the reinforcement, also in megapascals (MPa); d_{eq} is the equivalent diameter of the longitudinal reinforcement within the tensile zone, measured in millimeters (mm).

The coefficient for non-uniform strain in tensile reinforcement is determined

using Equation (2):

$$\psi = 1.1 - 0.65\frac{f_{tk}}{\rho_{te}\sigma_s} \tag{2}$$

where: f_{tk} represents the axial tensile strength of the concrete measured in MPa, and ρ_{te} denotes the ratio of longitudinal tensile reinforcement.

4. Computational Model and Material Parameters

4.1. Model Establishment

In this study, MIDAS software is employed to develop a three-dimensional finite element numerical model representing the tunnel site area, simulating the construction conditions. The model is used to evaluate the deformation and stress responses of the existing railway structure situated above the tunnel, both prior to and following the tunnel's construction. This evaluation aims to assess the impact of the newly constructed structure on the safety of the existing infrastructure. The excavation's influence range is considered to be 3 to 5 times the tunnel diameter [13] [14]. To mitigate boundary effects, the model dimensions are defined as 200 m × 200 m × 80 m, encompassing 124,646 elements and 69,881 nodes. Figure 2 illustrates the three-dimensional numerical model. In the numerical model, the ideal elastoplastic constitutive model is adopted for the rock and soil materials, following the Mohr Coulomb strength criterion. The linear elastic constitutive model is adopted for structures such as tunnel segments, roadbeds, and frame bridges, without considering the influence of groundwater and surrounding rock structural planes.

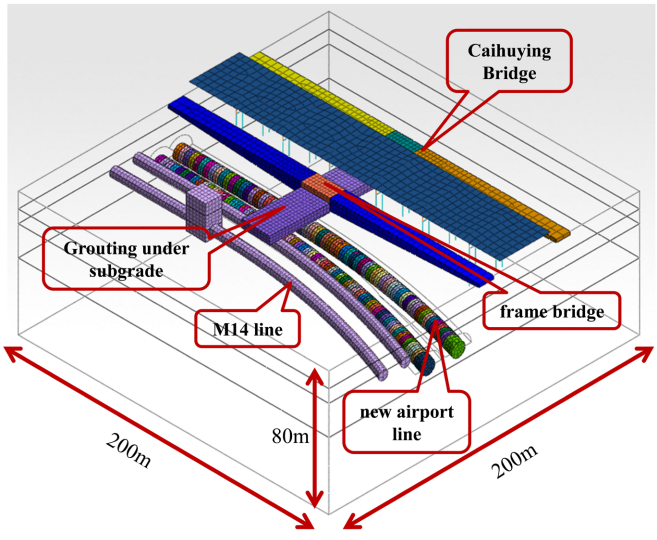

Figure 2. Three-dimensional numerical simulation model.

4.2. Design of Calculation Steps

In accordance with the construction organization plan, the sequence of engineering operations is as follows: first, the Caihuying Bridge is constructed, followed by

the railway frame bridge culvert, then the M14 line, and finally the proposed shield tunnel section. Prior to the shield tunnel construction, the stratum will be reinforced using subgrade sleeve valve pipe grouting and segment grouting. This is intended to enhance the self-stability of the surrounding rock and minimize the impact of the proposed construction on existing structures. To illustrate the effectiveness of the grouting reinforcement, the model calculations are performed for both non-grouting and grouting scenarios, as outlined in Table 3.

Table 3. Construction sequence.

Construction Sequence	Non-Grouting Condition	Grouting Condition	Remarks
1	Initial ground stress balance	Initial ground stress balance	Zero displacement of surrounding rock
2	Caihuying bridge construction	Caihuying bridge construction	/
3	Frame bridge culvert construction	Frame bridge culvert construction	/
4	M14 line construction	M14 line construction	Zero displacement of surrounding rock
5	Left line excavation	Subgrade grouting	/
6	Completion of left line excavation	Left line excavation	/
7	Right line excavation	Left line segment grouting	/
8	Completion of right line excavation	Completion of left line excavation	/
9		Right line excavation	/
10		Right line segment grouting	/
11		Completion of right line excavation	/

4.3. Calculation Parameters

Based on the geological survey data, the stratigraphic sequence in the engineering area is, from top to bottom: silty clay, pebble layer 5, pebble layer 7, and conglomerate layer. The mechanical parameters of rock and soil mass are selected based on the geological survey report and industry standards. The parameters for the model materials are presented in Table 4.

Table 4. Model material parameters.

Material	Density (g/cm^3)	Cohesion (kPa)	Internal Friction Angle (˚)	Elastic Modulus (MPa)	Poisson's Ratio
Silty Clay	1.84	34	16	4.2	0.35
Pebble 5	2.1	0	27	60	0.34
Pebble 7	2.11	0	32	80	0.32
Conglomerate	2.13	0	38	140	0.3
C35	2.5	/	/	31,500	0.2
C40	2.5	/	/	32,500	0.2
C50	2.5	/	/	34,500	0.2

5. Numerical Analysis

5.1. Deformation Patterns of Railway Subgrade

In MIDAS, both stratum and structural deformations are considered positive if they are in the same direction as the coordinate axis; thus, settlement deformations are negative, while uplift deformations are positive. To more intuitively reflect the impact of tunnel construction on the deformation of existing structures, an analysis is conducted at the cross-section where the shield tunnel underpasses the railway using a slicing method. Additionally, the displacement of the computational model is reset to zero before tunnel excavation.

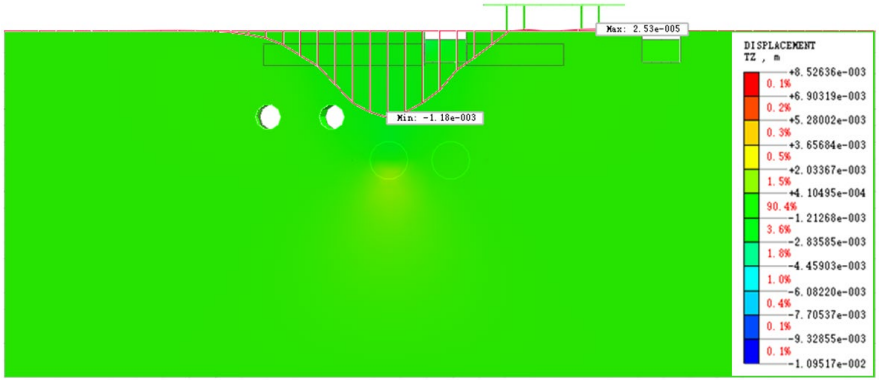

(a) Deformation contour map of the subgrade under non-grouting conditions

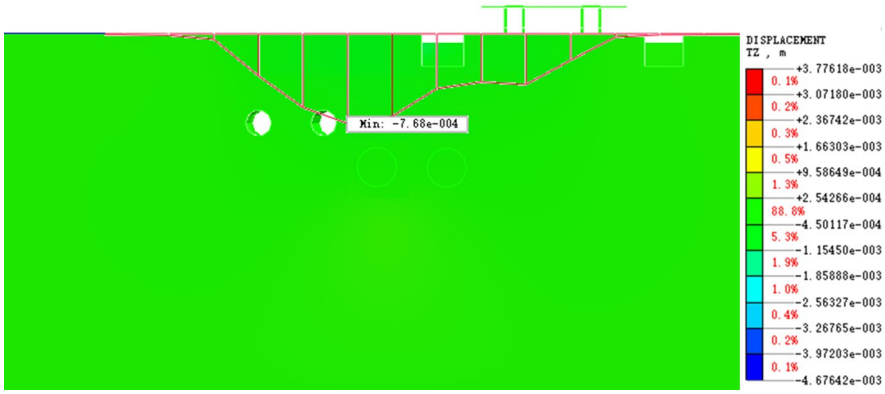

(b) Deformation contour map of the subgrade under grouting conditions

Figure 3. Contour maps depicting structural deformation before the left line tunnel excavation reaches the subgrade section (unit: m).

Upon excavating the left line tunnel to directly beneath the railway subgrade, the deformation of the existing subgrade structure is depicted in **Figure 3**. In scenarios without grouting, the maximum settlement deformation of the railway subgrade above is observed to be 1.18 mm, situated directly over the left line tunnel and distanced from the tunnel's outline. The settlement deformation of the subgrade diminishes, forming an overall "concave" curve distribution, aligning with Peck's theoretical framework [15]. Following grouting reinforcement of the stratum beneath the subgrade, the pattern of subgrade settlement deformation remains

unchanged. However, the magnitude of deformation decreases, with the maximum settlement deformation still occurring directly above the left line tunnel, now reduced to 0.77 mm.

Following the passage of the left-line tunnel through the railway subgrade, the deformation behavior of the existing subgrade structure is depicted in Figure 4. Under conditions without grouting, the maximum settlement deformation of the existing railway subgrade at this stage reaches 2.10 mm, occurring directly above the left line. The settlement deformation of the subgrade continues to exhibit a "concave" curve distribution, which is steeper compared to the previous stage. Under grouting conditions, the deformation pattern remains unchanged, with the maximum settlement deformation reduced to 1.11 mm.

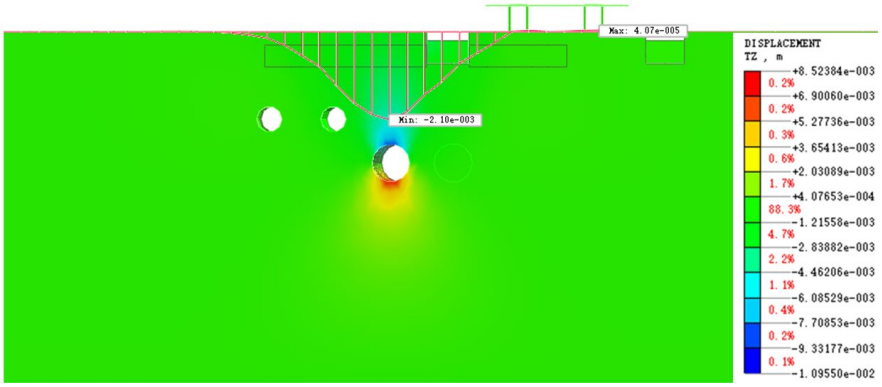

(a) Contour map of subgrade deformation under non-grouting conditions

(b) Contour map of subgrade deformation under grouting conditions

Figure 4. Contour map illustrating structural deformation after the left line tunnel traverses the subgrade section (unit: m).

As the excavation of the right line tunnel progresses to directly beneath the railway subgrade, the deformation behavior of the existing subgrade structure is depicted in Figure 5. Under conditions without grouting, the maximum settlement point of the railway subgrade shifts towards the right line tunnel, exhibiting a maximum deformation of 3.25 mm. The settlement deformation continues to follow a "concave" curve pattern. Conversely, with grouting applied, the maximum settlement deformation of the railway subgrade reduces to 1.70 mm. Although the

deformation pattern remains largely similar to the non-grouted condition, the "concave" curve's extent is broader and the curve itself is relatively smoother.

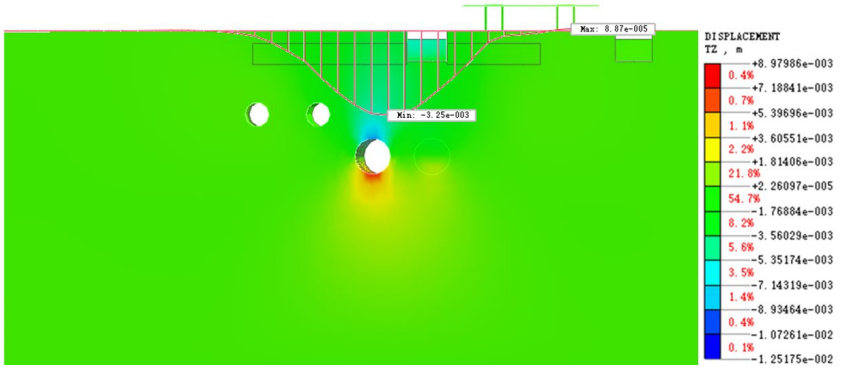

(a) Contour map of subgrade deformation under non-grouting conditions

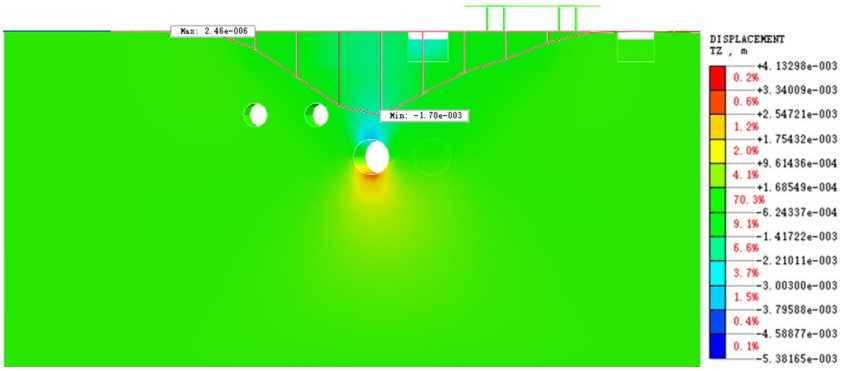

(b) Contour map of subgrade deformation under grouting conditions

Figure 5. Illustrates the deformation contour map of the structure prior to the excavation of the right line tunnel reaching the subgrade section (unit: m).

Following the crossing of the right-line tunnel through the railway subgrade, the deformation characteristics of the existing subgrade structure are illustrated in **Figure 6**. Under non-grouting conditions, the maximum settlement of the railway subgrade shifts towards the right-line tunnel, positioned approximately at the midpoint between the two lines, with a peak deformation of 4.64 mm. When grouting is applied, the maximum settlement deformation reduces to 2.08 mm. Although the deformation pattern remains largely similar to that observed without grouting, the "concave" curve extends over a broader range and is less pronounced. In both scenarios, the deformation of the subgrade structure remains below the control threshold, thereby complying with the specified standards.

Figure 7 illustrates the progression of subgrade settlement deformation under various operating conditions. As the shield tunnel advances incrementally, the deformation of the existing subgrade structure increases progressively. A notable surge in settlement deformation occurs when the tunnel approaches and traverses the subgrade section. Once the tunnel has passed and moved away, the deformation curve transitions from steep to more gradual. Upon the completion of the tunnel section, the subgrade settlement deformation reaches its peak. Comparatively,

the implementation of grouting significantly mitigates the impact of shield tunnel excavation on the vertical displacement of the subgrade. Following the completion of the right tunnel section, the cumulative subgrade settlement deformation is reduced to merely 45% of that observed under non-grouting conditions. The use of grouting reinforcement measures effectively aids in controlling the deformation of existing railway structures.

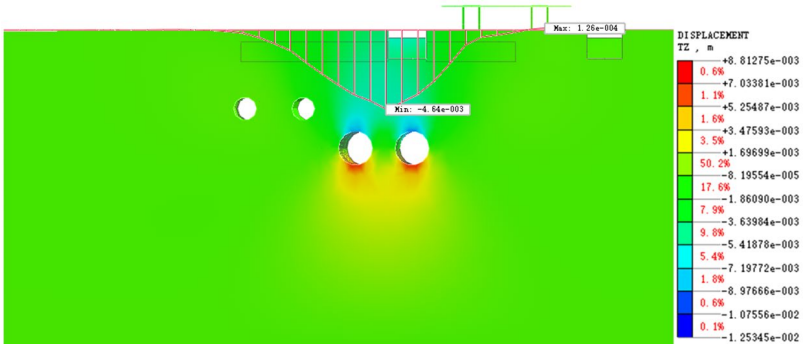

(a) Contour map of subgrade deformation under non-grouting conditions

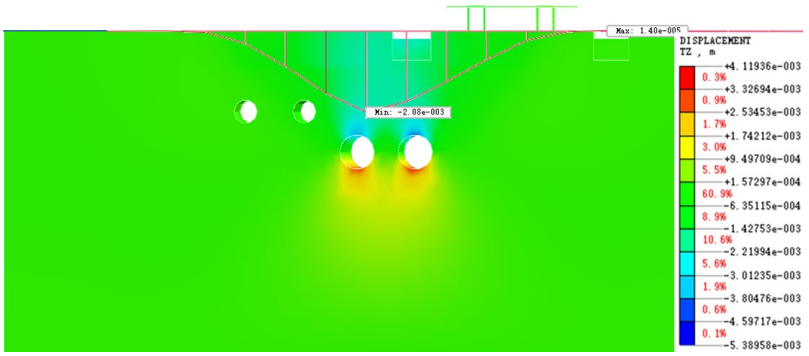

(b) Contour map of subgrade deformation under grouting conditions

Figure 6. Deformation contour map of the structure after the right-line tunnel traverses the subgrade section (unit: m).

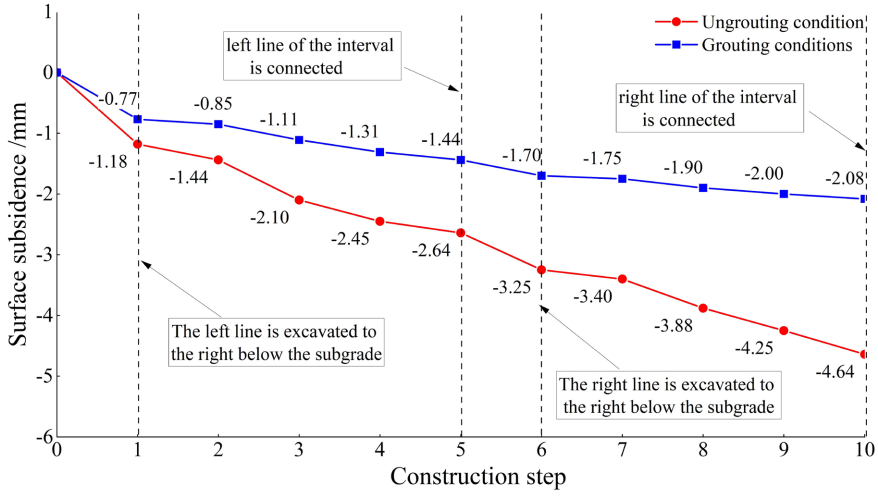

Figure 7. Illustrates the progression of subgrade settlement deformation (measured in mm).

5.2. Analysis of Structural Safety for Frame Bridges and Culverts

Upon the completion of the proposed tunnel section, the deformation behavior of the railway frame bridge and culvert structures is depicted in Figure 8. Without grouting, the maximum deformation observed in the existing bridge and culvert structures is 4.68 mm, occurring at the side wall adjacent to the newly constructed shield tunnel, indicating an overall settlement deformation. With grouting, the maximum deformation reduces to 2.07 mm, with a deformation pattern similar to the non-grouting scenario. In both scenarios, the deformation values remain below the 5 mm control limit, ensuring that the structural deformation complies with the specified standards.

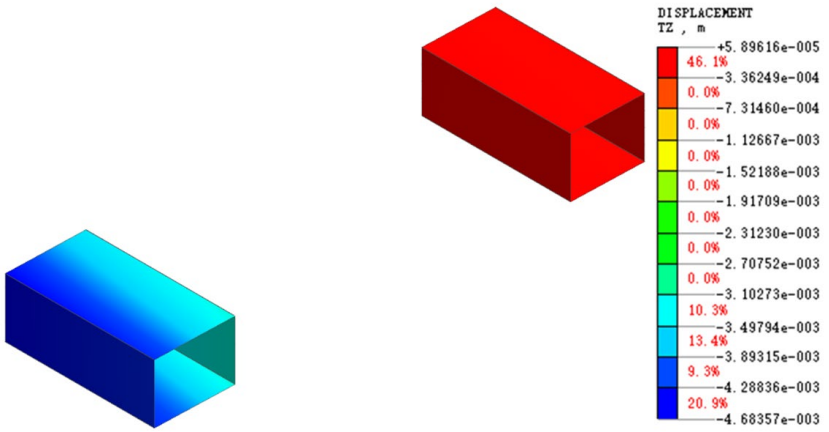

(a) Deformation contour map of bridge and culvert structures under non-grouting conditions

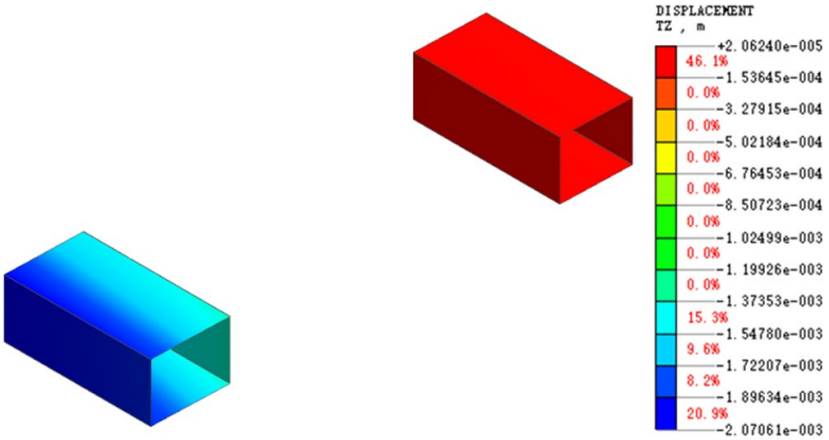

(b) Deformation contour map of bridge and culvert structures under grouting conditions

Figure 8. Deformation contour map of bridge and culvert structures following the completion of the proposed tunnel (unit: mm).

Following the completion of the interval tunnel construction, the bending moment distribution of the railway frame bridge culvert is illustrated in Figure 9. Under non-grouting conditions, the existing bridge culvert structure experiences a maximum tensile force of 555.09 kN·m on the outer side, located at the side wall

adjacent to the newly constructed shield tunnel. The maximum tensile force on the inner side is 464.52 kN·m, positioned at the bottom slab. The structure's top and bottom slabs are subjected to tensile forces on the inner side, whereas the side walls experience tensile forces on the outer side. When grouting is applied, the internal force distribution of the bridge culvert structure remains largely unchanged from the non-grouting scenario. The maximum tensile force on the outer side is reduced to 551.90 kN·m, and on the inner side to 447.66 kN·m, indicating a slight difference in magnitude.

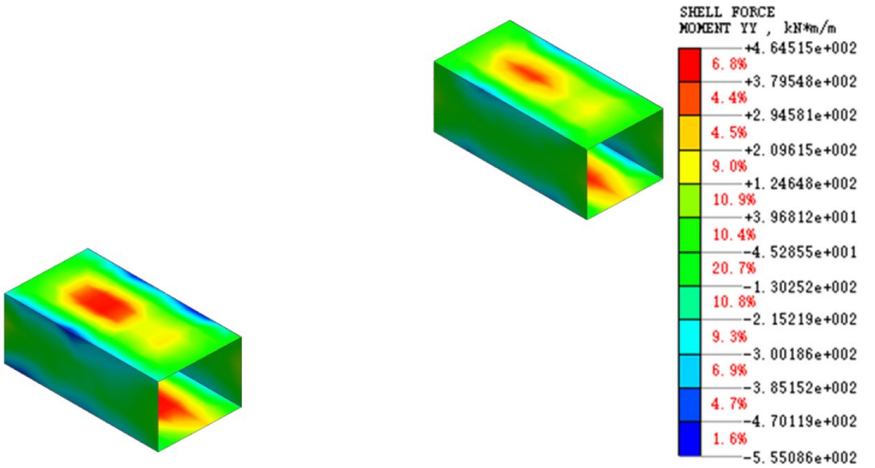

(a) Bending moment distribution diagram of bridge and culvert structures under non-grouted conditions

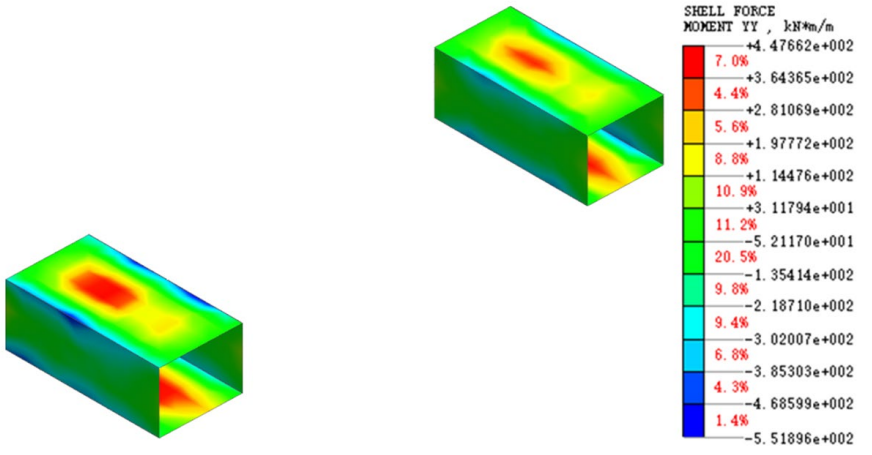

(b) Bending moment distribution diagram of bridge and culvert structures under grouted conditions

Figure 9. Bending moment distribution diagrams of bridge and culvert structures following the completion of the proposed tunnel (unit: kN·m).

In the inspection and calculation process of frame bridges, each meter of length is considered as a unit for analysis. The evaluation of both the ultimate load-bearing capacity and the normal service limit states is conducted based on pure bending components, as detailed in **Table 5** and **Table 6**.

Table 5. Crack inspection calculation for box girder bridges.

Condition	Location	Calculated Value (mm)	Control Value (mm)	Inspection Outcome
Without Grouting	Top Slab	0.178	2	Pass
	Bottom Slab	0.073	2	Pass
With Grouting	Top Slab	0.176	2	Pass
	Bottom Slab	0.070	2	Pass

Table 6. Load-bearing capacity verification table for box girder bridge.

Condition	Location	Calculated Reinforcement (mm^2)	Designed Reinforcement (mm^2)	Verification Result
Non-grouted	Top Slab	3163	4710	Qualified
	Bottom Slab	2853	6280	Qualified
Grouted	Top Slab	3143	4710	Qualified
	Bottom Slab	2807	6280	Qualified

Table 5 and Table 6 reveal that in both grouted and non-grouted scenarios, following the construction of the shield tunnel underpass, the most critical section of the existing railway frame bridge structure is found at the top slab. The crack width and reinforcement area comply with the regulatory standards, ensuring structural safety. Comparatively, with grouting reinforcement, the internal forces within the structure decrease, resulting in narrower crack widths and a reduced calculated requirement for reinforcement area.

6. Engineering Practice

To prevent damage to the existing subgrade structure during the construction of the shield tunnel segment, reinforcement measures such as subgrade sleeve valve pipe grouting and segment grouting were implemented on-site. Concurrently, real-time monitoring and measurements were conducted at section K4+819, where the tunnel passes beneath the subgrade. 9 settlement observation points are set up along the vertical tunnel axis on the surface of the roadbed. When measuring the distance between the cross-section and the tunnel excavation face from 2D to 5D, observation records are taken every 2 days; Observe and record every day within the range of 1D to 2D; Observe and record every 0.5 days within the 1D range. According to the dynamic feedback of roadbed settlement and deformation monitoring data during the construction phase of the interval tunnel underpass, the time history curve of roadbed deformation at the observation point directly above the tunnel on section K4+819 is shown in Figure 10. Construction adjustments were made dynamically in response to the monitoring data on subgrade settlement and deformation during the tunnel construction phase. The time-history curve illustrating subgrade deformation at section K4+819

is presented in Figure 10.

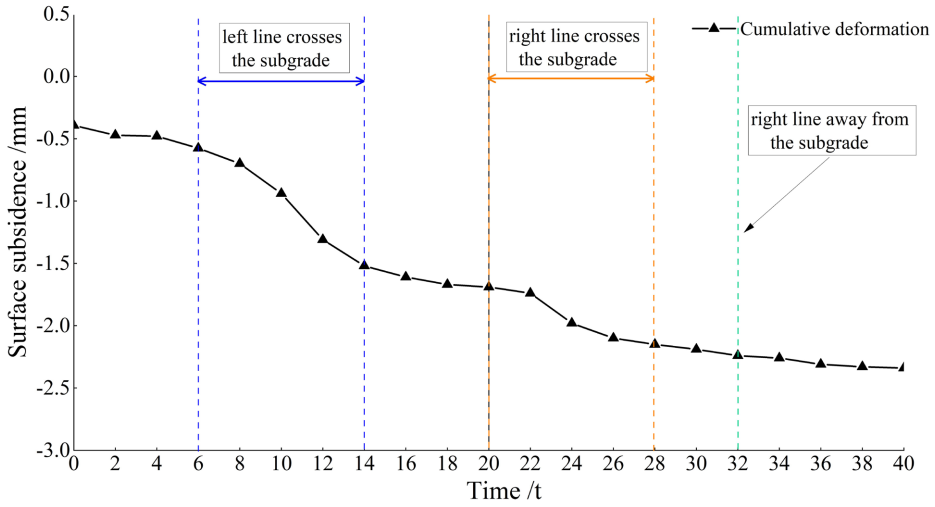

Figure 10. Illustrates the time history curve of settlement at the K4+819 cross-section of the roadbed.

According to Figure 10, as the construction progresses, the roadbed experiences a gradual increase in settlement deformation. A significant increase in settlement is observed when the shield tunnel approaches and passes through the roadbed cross-section. Once the tunnel moves beyond the roadbed section, the settlement deformation curve transitions from steep to more gradual. The observed on-site monitoring data and the results from numerical simulations are largely consistent in terms of the overall deformation trends of the structure. After the right-line tunnel moves away from the cross-section, the deformation of the existing railway roadbed stabilizes, with a final settlement value of 2.33 mm. The deviation from the numerical simulation is 10.7%, which is considered acceptable within the engineering context. This demonstrates that finite element modeling effectively simulates the construction of a deep cutting roadbed over an existing tunnel, accurately reflecting real-world engineering scenarios. The slurry is made of water glass grout, which has a significant grouting effect and no pollution to the environment. To prevent surface uplift, low-pressure slow grouting measures are taken during grouting, and there is basically no uplift deformation on the surface after grouting is completed.

7. Conclusion

1) The construction of shield tunnels beneath existing railway subgrades induces settlement deformation, characterized by a “concave” curve distribution. Settlement deformation is more pronounced closer to the tunnel’s contour and diminishes with distance from it. As construction progresses, the settlement deformation of the subgrade increases. When the tunnel approaches and passes directly beneath the subgrade, the deformation curve transitions from a gentle to a steep slope. Once the tunnel has passed and moved away, the curve reverts from

steep to gentle. The maximum settlement deformation of the subgrade is observed upon the completion of the tunnel section.

2) Following grouting reinforcement, the settlement deformation of the subgrade continues to exhibit a "concave" curve distribution; however, the curve is less pronounced and the distribution range is broader. Prior to implementing grouting measures, the maximum subgrade settlement was recorded at 4.64 mm. Post-grouting reinforcement, the maximum settlement deformation was reduced to 2.08 mm. Grouting reinforcement of the stratum effectively mitigates the impact of shield tunneling on the existing railway, thereby controlling subgrade settlement efficiently. Engineering practice has confirmed the precision of numerical calculations, ensuring that subgrade settlement deformation adheres to control standards.

3) Without grouting, the construction of the shield tunnel underpass results in the most critical section of the railway frame bridge structure being located at the top slab, with a maximum crack width of 0.178 mm. Grouting reinforcement improves the structural stress environment, resulting in narrower crack widths and a reduced required reinforcement area. The structural safety under both conditions satisfies the necessary requirements.

Conflicts of Interest

The author declares no conflicts of interest regarding the publication of this paper.

References

[1] Kim, S., Park, J., Duong, D.L., Cho, S., Kim, S.W. and Yang, H. (2019) Proximity Engineering of the Van Der Waals Interaction in Multilayered Graphene. *ACS Applied Materials & Interfaces*, **11**, 42528-42533. https://doi.org/10.1021/acsami.9b16655

[2] Dai, X.P., Guo, T. and Qin, J.S. (2006) Research on Minimum Depth Burial of Shield Tunnel Machines Crossing over Ground Base under Rivers. *Rock and Soil Mechanics*, **27**, 782-786.

[3] Shang, X., Miao, S., Wang, H., Yang, P. and Xia, D. (2025) A Prediction Model for Surface Settlement during the Construction of Variable Cross-Section Tunnels under Existing Structures Based on Stochastic Medium Theory. *Tunnelling and Underground Space Technology*, **155**, Article ID: 106177. https://doi.org/10.1016/j.tust.2024.106177

[4] Liu, B., Xi, D. and Xu, P. (2019) Study on the Interaction of Metro Shield Tunnel Construction Under-Crossing the Existing Longhai Railway. *Geotechnical and Geological Engineering*, **38**, 2159-2168. https://doi.org/10.1007/s10706-019-01154-y

[5] Xu, G.C., Hu, P. and Li, C.X. (2010) Influence Analysis on a Subway Shield Tunnel Crossing below a High Speed Railway. *Stand Alone*, **2010**, 519-527.

[6] Lou, G.C. and Wang, S.D. (2011) Study on Settlement of Highway Bed Due to Underground Construction of Crossing Railway Tunnels. *Applied Mechanics and Materials*, **90**, 1846-1852. https://doi.org/10.4028/www.scientific.net/amm.90-93.1846

[7] Song, Y.G. (2022) Study on Settlement and Deformation Characteristics of Subway Shield Tunnel Penetrating High Speed Railroad Foundation. *Railway Survey*, **48**,

107-113.

[8] Wu, B., Lin, X., Su, D., Han, K. and Chen, X. (2024) Settlement Transfer Mechanism of CFG Piles for Strengthening High-Speed Railway Subgrades Induced by Twin Shield Tunnelling Undercrossing. *Tunnelling and Underground Space Technology*, **145**, Article ID: 105577. https://doi.org/10.1016/j.tust.2023.105577

[9] Song, M., Liu, J., Wang, X., Lou, H. and Lin, X. (2022) Study on Railway Subgrade Settlement Induced by an Ultra-Large-Diameter Shield Tunnel Crossing under Railway Subgrade. *Symmetry*, **15**, Article 75. https://doi.org/10.3390/sym15010075

[10] Huang, Z., Zhang, H., Long, Z., Qiu, W., Meng, G. and Zhu, L. (2020) Field Test Optimization of Shield Tunnelling Parameters Undercrossing an Existing High-Speed Railway Tunnel: A Case Study. *Geotechnical and Geological Engineering*, **39**, 1381-1398. https://doi.org/10.1007/s10706-020-01564-3

[11] Wang, L. (2015) Settlement Impact Analysis and Countermeasure Research of the down Traversing Formed by the Double-Arch Subway Tunnels through the Existing Railways in Loess Area. *MATEC Web of Conferences*, **22**, Article ID: 04006. https://doi.org/10.1051/matecconf/20152204006

[12] Zheng, M.X., Chen, Y.Q. and Ou, Y.L. (2014) Numerical Analysis on the Subgrade Settlements in Case of Different Tunneling Excavation Plans across Railway. *Applied Mechanics and Materials*, **488**, 424-428. https://doi.org/10.4028/www.scientific.net/amm.488-489.424

[13] Huang, X., Schweiger, H.F. and Huang, H. (2013) Influence of Deep Excavations on Nearby Existing Tunnels. *International Journal of Geomechanics*, **13**, 170-180. https://doi.org/10.1061/(asce)gm.1943-5622.0000188

[14] Qiao, L.T., Kang, W. and Wen, Q. (2022) Experimental Study on Anchor Characteristics of Shallow Buried Layered Soft Rock Tunnel in Deep Graben. *Journal of Railway Engineering*, **39**, 47-52.

[15] Peck, E.R. (1983) Sellmeier Fits with Linear Regression; Multiple Data Sets; Dispersion Formulas for Helium. *Applied Optics*, **22**, 2906-2913. https://doi.org/10.1364/ao.22.002906